Bond-orientational structure and melting signature in krypton physisorbed onto graphite at complete coverage

M. W. Roth
Department of Natural Sciences, Texas A&M International University, 5201 University Boulevard, Laredo, Texas 78041
(Received 31 March 1997; revised manuscript received 2 February 1998)

A constant-temperature, constant-density molecular-dynamics method is utilized to study the bond-orientational structure and behavior in Kr-gr for the solid, fluid, and melting transition regimes at monolayer completion ($\rho=1$). Several bond-orientational order parameters are introduced to help monitor the system's symmetry behavior, both with respect to the substrate as well as intrinsic. The first- and fourth-neighbor shells exhibit random thermal fluctuations in the absence of significant interaction with other neighbor shells in the solid. The fluctuations magnify as temperature increases, promoting the decay of structural order through melting and into the fluid. The second and third shells exhibit not only thermal fluctuations but also interaction via local shared-lattice defects (vacancy/interstitial pairs) that begin in the low-temperature solid. Multiple-consecutive vacancies or interstitials are found to be far rarer in occurrence than single ones. The monolayer loses all bond-orientational order with respect to the graphite substrate upon melting, while floating (intrinsic) bond-orientational order in the lattice itself is maintained through the high-temperature fluid ($T\approx 250$ K). The intrinsic bond-orientational order of the fluid after melting is insensitive to change in temperature, and therefore local vacancy production does not increase with increasing temperature until the generation of vacancies created by the onset of desorption at $T\approx 200$ K. Finite-size scaling results show that the algebraic exponent for the order parameter OB6 reaches the critical value of $\eta_6=\frac{1}{4}$ simultaneously with the onset of melting around $T=100$ K illustrating that neither a hexatic phase nor an intermediate region is supported in the system in this study. [S0163-1829(98)07319-6]

I. INTRODUCTION

Quasi-two-dimensional (2D) melting continues to be an area of scientific interest. As theoretical and experimental resources have been continuously improving over the past decade, many research efforts in the field are products of renewed interest and revisitation of unresolved issues oftentimes accompanied with conflicting results. Such issues are, among others, the mechanism and order of the 2D melting transition.

Many analytical theories with a diverse variety of results describing possible melting mechanisms have been developed.[1–8] Some theories predict a first-order transition, while others describe second-order or higher transitions. One particular theory credited to Kosterlitz, Thouless, Halperin, Nelson, and Young (KTHNY) requires a two-stage melting scheme where the solid melts into a hexatic sixfold-symmetric bond-orientationally ordered fluid through dislocation pair unbinding and subsequently makes a transition at a higher temperature to an isotropic fluid via disclination pair unbinding.[4–6] The solid possesses long-range bond-orientational order and quasi-long-range translational order; the hexatic fluid has a short-range translational order but has quasi-long-range bond-orientational order and the isotropic fluid possesses short-range bond-orientational and translational order. In addition to KTHNY theory, Strandburg[2] outlines Chui's theory where grain-boundary related translational-order loss drives the melting mechanism for a single first-order transition. It is mainly from the fact that KTHNY theory is at odds with many experimental and computational results that so much interest has lately been focused on the order of the melting transition and the role of bond-orientational order loss in melting.

Currently, the order of melting and the nature of the melting transitions in real physisorbed systems as well as idealized 2D systems[9,10] are controversial issues. In fact, recent computer simulations and experiments do observe a hexatic phase and two-stage melting in a system of interacting dipoles.[11] Chen, Kaplan, and Mostoller have completed an interesting molecular dynamics (MD) computer simulation of a Lennard-Jones system using as many as 102 400 atoms and observed a metastable hexatic phase existing between solid and fluid.[12] In addition, a smaller system in the solid phase melted when the system was made larger, which is an indication of the influence of long-range correlations being important for second-order phase transitions.[12] On the other hand, new studies of melting in 2D quantum systems report a first-order-type transition.[13] Naidoo and Schnitker conducted a MD study of r^{-12} repulsive particles and concluded that some aspects of first-order melting were present (two-phase coexistence) as well as a hexaticlike phase.[14] This work also examined the sensitivity of results on initial conditions and adequate phase-space sampling. Zollweg[15] and McTague, Frenkel, and Allen[16] studied the bond-orientational behavior of 2D hard disk and r^{-6} repulsive systems, respectively, and presented results for the oriented and isotropic fluids in general agreement with KTHNY theory. Weber and Marx[17] present a study involving scaling of the bond-orientational order parameters and behavior of Binder's cumulant for the hard-disk melting transition that favors a first-order melting transition. Aoiki and Yonezawa[18] report an MD study of sixfold bond-orientational order in a system of repelling spherocylinders. The system went from a solid to a smectic

phase, which was a result of interacting hexatic layers. Some recent experimental work deals with sixfold bond-orientational order-parameter scaling near the hexatic-liquid phase transition,[19] optical anisotropy in long-chain molecules from molecular tilt[20] and a continuous hexatic to liquid-melting transition in magnetic-bubble lattices.[21]

Although there are some very interesting physical systems under examination both theoretically[9–18] and experimentally,[19–21] rare gas monolayers physisorbed onto a graphite substrate have proved to be readily accessible real systems to which computational models and analytical formalisms may be applied. The Kr-gr system is chosen for this work because it exhibits a rich and interesting phase diagram, the potentials describing the interactions of the system components are well known, and the system enjoys a wealth of experimental data.

The phase diagram of Kr-gr has been thoroughly studied and mapped out.[22] A strong first-order melting transition is found at submonolayer coverages. This transition becomes more second-orderlike as the coverage ρ is increased towards completion (in units of 0.0636 atoms/Å^2). The solid-solid commensurate-incommensurate transition, which occurs for $\rho>1$, involves a relatively complicated domain wall structure as well as a reentrant,[23] or domain wall[22] fluid and is more continuous[24] than submonolayer transitions. Studies of the fluid-registered solid transition include vapor-pressure isotherm work. From these investigations, the transition is determined to be first order up to 115 K.[24] The reentrant melting of Kr-gr is rather complicated;[25] a renormalization-group treatment has been put forth[26] using vacancy and domain-wall network arguments to explain the melting mechanism. The submonolayer melting transition is found to be first-orderlike, while the complete monolayer transition appears to be more continuous; no hexatic phase has yet been observed.

The purpose of this work is not only to better understand the bond-orientational structure of the Kr-gr solid and fluid monolayer, but also to understand the behavior of and changes in the system's bond-orientational structure and symmetry as related to its dynamics.

II. COMPUTATIONAL APPROACH AND INTERACTION POTENTIALS

A ($N=256$, $\rho=1$, T) MD scheme with periodic-boundary conditions (PBCs) is utilized. The computational cell is a rhombic prism with sides $\mathbf{a}=(68.16\ \text{Å},0,0)$, $\mathbf{b}=(34.08\ \text{Å},59.03\ \text{Å},0)$, and $\mathbf{c}$ being perpendicular to the (x,y) plane. The cell is oriented with $\mathbf{a}$ and $\mathbf{b}$ being along the $\hat{x}$ and $\hat{y}$ directions of the graphite-basal plane, respectively; the oblique coordinate system rigidly attached to the graphite substrate is well known and standard. PBCs are maintained in the (x,y) plane by repeating the box eight times so it is surrounded by copies of itself before any lattice sums or parameter calculations are done; free-boundary conditions are implemented in the $\hat{z}$ direction in order to allow for the possibility of desorption. The equations of motion are integrated utilizing a second-order predictor-corrector scheme; the time step is $\Delta t=0.004$ ps, which yields energy conservation to within about 1% throughout the total simulation time. Typical runs are taken out for about 10^4 time steps in order to eliminate initial transients or bottlenecks, and pertinent sums for calculation of various parameters is taken out for roughly the next 5×10^4 time steps. Neighbor lists are utilized in order to maximize computational efficiency. Some mention will later be made of the effect of computational cell size as well as different boundary conditions.

The two important types of interactions considered are krypton-krypton (Kr-Kr) and krypton-graphite (Kr-gr) interactions. The Kr-Kr interaction is of the Lennard-Jones (LJ) form:

$$U_{ij}=4\epsilon\left[\left(\frac{\sigma}{r_{ij}}\right)^{12}-\left(\frac{\sigma}{r_{ij}}\right)^{6}\right]. \tag{1}$$

Here $U_{ij}=U_{ij}^{\text{Kr-Kr}}$ is the potential energy of interaction between adatom (i) and adatom (j), $(\epsilon,\sigma)=(\epsilon_{\text{Kr-Kr}},\sigma_{\text{Kr-Kr}})=(171\ \text{K},3.60\ \text{Å})$ are the potential parameters, and r_{ij} is the distance separating the two relevant atoms.

The Kr-gr interaction $U_{ij}^{\text{Kr-gr}}$ is derived from a krypton-carbon (Kr-C) atom-atom interaction between krypton atom (i) and carbon atom (j), which is of the LJ form as in Eq. (1) with $(\epsilon,\sigma)=(\epsilon_{\text{Kr-C}},\sigma_{\text{Kr-C}})=(31.3\ \text{K},3.36\ \text{Å})$. To avoid a computationally intense lattice sum, Steele[26] takes advantage of the graphite-substrate symmetry in a well-known and widely used Fourier expansion:

$$U_i^{\text{Kr-gr}}=E_{0i}(z_i)+\sum_{n=1}^{\infty}E_{ni}(z_i)f_n(x_i,y_i). \tag{2}$$

Here $U_i^{\text{Kr-gr}}$ is the potential energy of interaction between krypton atom (i) having spatial coordinates (x_i,y_i,z_i) in an orthogonal Cartesian coordinate system rigidly attached to the substrate with its origin at a graphite hexagon center, and the substrate. The E_{ni} are the laterally averaged interaction terms and the $f_n(x_i,y_i)$ are periodic functions representing the lateral undulation in the interaction present due to the graphite basal-plane symmetry. The series converges rapidly, so the only term retained from the expansion in Eq. (2) is $n=1$. In addition to the Fourier transform on one graphite plane, the potentials are subsequently summed over an infinite number of graphite planes. The analytical forms for the terms contained in Eq. (2) are

$$E_{0i}(z_i)=\frac{2\pi q\epsilon_{\text{Kr-C}}\sigma_{\text{Kr-C}}^6}{a_s}\left\{\frac{2\sigma_{\text{Kr-C}}^6}{45d(z_i+0.72d)^9}-\frac{1}{z_i^4}-\frac{2z_i^2+7z_id+7d^2}{6d(z_i+d)^5}\right\}, \tag{3}$$

$$E_{ni}(z_i)=\frac{2\pi\epsilon_{\text{Kr-C}}\sigma_{\text{Kr-C}}^6}{a_s}\left\{\left(\frac{\sigma_{\text{Kr-c}}^6}{30}\right)\left(\frac{g_n}{2z_i}\right)^5K_5(g_nz_i)-2\left(\frac{g_n}{2z_i}\right)^2K_2(g_nz_i)\right\}, \tag{4}$$

and

$$f_1(x_i,y_i)=f_n(x_i,y_i)|_{n=1}=-2\left\{\cos\frac{2\pi}{a}\left[x+\left(\frac{y}{\sqrt{3}}\right)\right]+\cos\frac{2\pi}{a}\left[x-\left(\frac{y}{\sqrt{3}}\right)\right]+\cos\frac{4\pi}{a}\left(\frac{y}{\sqrt{3}}\right)\right\}. \quad (5)$$

In Eqs. (3)–(5), $a_s=5.24$ Å^2 is the area of the graphite unit cell, $d=3.37$ Å is the spacing between graphite planes, the K_i are modified Bessel functions of the second kind and of order i, and the g_n are the moduli of the nth reciprocal lattice vector of the substrate.[26]

For implementation using the MD method, the force on adsorbate atom (i) is calculated from the spatial gradient of the interaction energies:

$$\mathbf{F}_i(\mathbf{r}_i)=-\boldsymbol{\nabla}_i\left\{\sum_{j=1}^{N}U_{ij}^{\text{Kr-Kr}}(\mathbf{r}_i,\mathbf{r}_j)\left[1-\theta\left(\frac{r_{ij}}{r_c}\right)\right](1-\delta_{i,j})+U_i^{\text{Kr-gr}}(\mathbf{r}_i)\right\}. \quad (6)$$

Here θ is the Heaviside step function and a reflection of the fact that the lattice sum in the first term is truncated after a cutoff radius of $r_c=9$ Å. Also, $\delta_{i,j}$ is the Kroneker δ function and the part of the first term that contains it is present to reflect the fact the lattice sum cannot contain atom (i).

III. RESULTS

Several thermodynamic and structural parameters are good indicators of melting in physisorbed systems. Although thermodynamic data are studied for the melting transition of interest here, they are not presented now; their main usefulness is twofold. First, it is necessary to ensure that the point of maximum loss of translational order indeed coincides with maximum specific heat and, hence, that the MD runs exhibit convergence. In addition it is important to compare the thermodynamic melting signature of the system with other previous theoretical and experimental work. Such comparisons are favorable.

To help tie together the dynamics of the melting transition and the bond-orientational behavior, two translational-order parameters are monitored as functions of temperature. The first is

$$O1=\frac{1}{6N}\sum_{i=1}^{N}\left\langle\sum_{s=1}^{6}e^{i\mathbf{g}_s\cdot\mathbf{r}_i}\right\rangle. \quad (7)$$

Here the sum over (s) runs over all six reciprocal lattice vectors $\mathbf{g}_s$ for the graphite substrate and $\mathbf{r}_i$ locates adsorbate atom (i) in the orthogonal Cartesian coordinate system mentioned earlier. $O1$ is an indicator of the translational order of the adsorbate with respect to the substrate, with $O1=1$ for a static, commensurate overlayer and $O1=0$ for either an infinite incommensurate lattice, or for the adsorbate atoms uniformly sampling positions in the (x,y) plane. $O1$ alone, however, is not sufficient to indicate melting, as it shows no unique signature of adatom-adatom fluctuations and could vanish even for a floating monolayer. The order parameter $O2$ is defined by

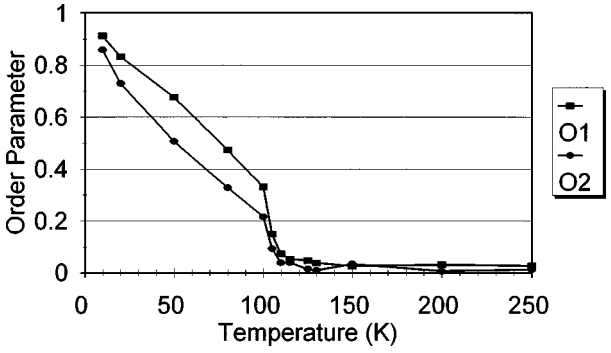

FIG. 1. Order parameters $O1$ and $O2$ as functions of temperature. Squares indicate $O1$ and circles indicate $O2$; uncertainties are on the order of ±0.03 before melting, ±0.08 during melting, and ±0.03 in the fluid. All points are connected by straight lines as a visual aid.

$$O2=\frac{1}{(3N)(N-1)}\sum_{i=1}^{N}\sum_{j=i+1}^{N}\left\langle\sum_{s=1}^{6}e^{i\mathbf{k}_s\cdot\mathbf{r}_{ij}}\right\rangle. \quad (8)$$

Here the $\mathbf{k}_s$ are the six reciprocal lattice vectors for a static $\sqrt{3}\times\sqrt{3}R30°$ adsorbate lattice and $\mathbf{r}_{ij}$ is the displacement vector between adatom (i) and adatom (j). $O2=1$ for a static, commensurate, adsorbate lattice and vanishes for either an infinite incommensurate lattice or for random sampling of positions in the (x,y) plane due to thermal atomic fluctuations. For both $O1$ and $O2$, angular brackets denote time averages. Together, $O1$ and $O2$ are excellent indicators of diminishing translational order and hence readily signal melting. For both $O1$ and $O2$, lattice sums are carried out to the fourth-nearest neighbors; $O1=O1(T)$ and $O2=O2(T)$ are presented in Fig. 1.

Bond-orientational order with respect to the substrate, as well as with respect to the adsorbate itself, is monitored. The bond-orientational order parameters OBn are defined by

$$OBn=\frac{\sum_{i=1}^{N}\sum_{j=1}^{N}\langle\cos(n\phi_{ij})f(r_{ij})(1-\delta_{i,j})\rangle}{\sum_{i=1}^{N}\sum_{j=1}^{N}\delta_{1,f(r_{ij})}}, \quad (9)$$

with

$$f(r_{ij})=\left\{\theta\left(\frac{r_{ij}}{R_A}\right)-\theta\left(\frac{r_{ij}}{R_B}\right)\right\}. \quad (10)$$

Here $\phi_{ij}=\cos^{-1}\{(x_j-x_i)/r_{ij}\}$ is the angle that the bond $\mathbf{r}_{ij}$ makes with the positive x axis. $f(r_i)$ reflects the fact that the OBn have been calculated separately for first- through fourth-nearest neighbors in the adsorbate lattice; R_A and R_B are the inner and outer cutoff radii, respectively, for the adjacent annular neighbor shells. Since there is nominal expansion in the registered lattice with temperature, the cutoff radii were taken to be the locations of the middle of the successive minima of the pair-distribution function of the low-temperature solid. Simply put, the neighbor shells are defined to be the successive peaks of the pair-distribution function, minimum to minimum. The denominator of Eq. (9) is

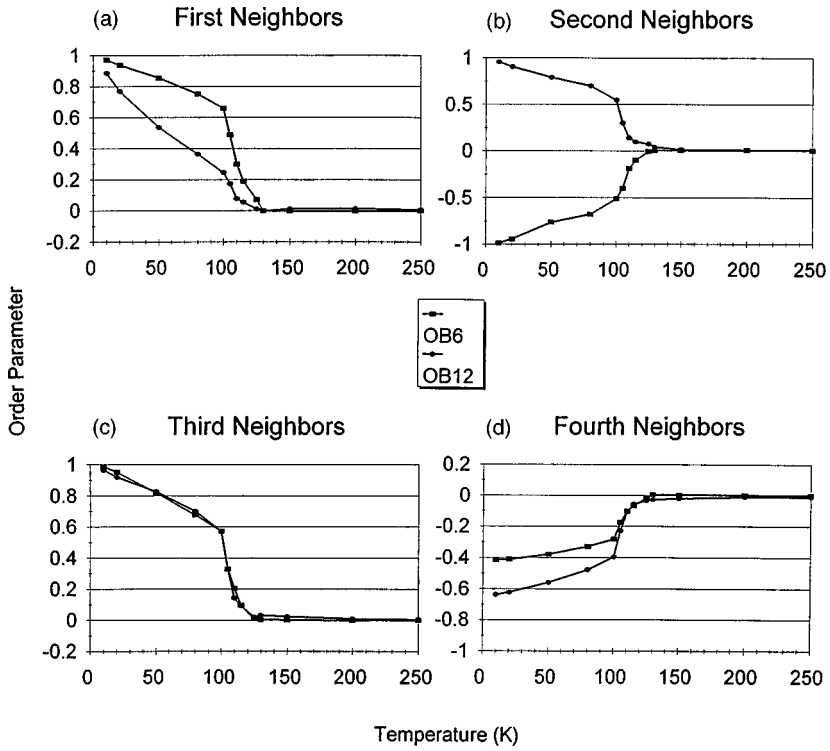

FIG. 2. Order parameters $OB6$ and $OB12$ as functions of temperature for first through fourth neighbors, respectively. Squares indicate $OB6$ and circles indicate $OB12$. Uncertainties are similar to those of $O1$ and $O2$. All points are connected by straight lines as a visual aid.

simply a counter of the number of bonds in consideration for the particular sum. The OBn are useful in studying the symmetry of the system as well as symmetry changes across melting, as they are more positive for greater population of $\phi_{ij}=2m\pi/n$, and more negative for greater population of $\phi_{ij}=(2m+1)\pi/n$, where m is a non-negative integer. The OBn vanish for uniform populations of ϕ_{ij}. Of course, the OBn can vanish for some nonuniform bond-angle distributions so it is important to examine order parameters for several different n in conjunction. $OB6=OB6(T)$ and $OB12=OB12(T)$ are the only two OBn exhibiting significant melting signatures. They are shown for first- through fourth-nearest neighbors in Figs. 2(a)–2(d), respectively. Their zero-temperature values as well as changes upon melting and their values at $T=250$ K (high-temperature fluid) are shown for first- through fourth-nearest neighbors in Table I.

The order parameters $OBRn$ are designed to measure bond-orientational order with respect to the krypton lattice. They are defined by

$$OBRn=\frac{\sum_{i=1}^{N}\sum_{j=1}^{N}\langle\cos(n\alpha_{ij})f(r_{ij})(1-\delta_{i,j})\rangle}{\sum_{i=1}^{N}\sum_{j=1}^{N}\delta_{1,f(r_{i,j})}}, \qquad (11)$$

with

$$\alpha_{ij}=\min_k\{(\phi_{ik}-\phi_{ij}):\phi_{ik}>\phi_{ij};f(r_{ik})f(r_{ij})=1\}. \qquad (12)$$

The $OBRn$ are similar to the OBn with the exception of the angles being included. Here the α_{ij} is the consecutive angle increasing counterclockwise (as guaranteed by $\phi_{ik}>\phi_{ij}$) between constituents of a particular neighbor shell [as ensured by $f(r_{ik})f(r_{ij})=1$] constructed with atom (i) at the center and the bond $\mathbf{r}_{ij}$ as the reference axis. $OBR6=OBR6(T)$ and $OBR12=OBR12(T)$ are shown for first- through fourth-nearest neighbors in Figs. 3(a)–3(d), respectively. The zero-temperature values as well as changes upon melting and the values at $T=250$ K for $OBRn$ with $n=1$, 2, 3, 4, 5, 6, and 12 are shown for first- through fourth-nearest neighbors in Table II.

Unnormalized bond-angle orientational distributions $P(\phi_{ij})$ are shown at various temperatures for Kr/gr in Figs. 4(a)–4(j). $P(\phi_{ij})$ is calculated by determining the frequency

TABLE I. Zero-temperature values, changes upon melting, and values at $T=250$ K for $OB6$ and $OB12$ evaluated for nearest through fourth-nearest neighbors moving vertically downward for a given parameter. Uncertainties are ±0.09 near melting and on the order of ±0.04 at $T=250$ K.

	$OB6$	$OB12$
	1	1
Zero-temperature	−1	1
value	1	1
	−0.5	−0.5
Change	−0.659	−0.245
upon	0.514	−0.506
melting	−0.567	−0.537
	0.287	0.369
	−0.0002	0.0076
Value at	0.0060	0.0072
$T=250$ K	0.001	0.0064
	0.0014	−0.0090

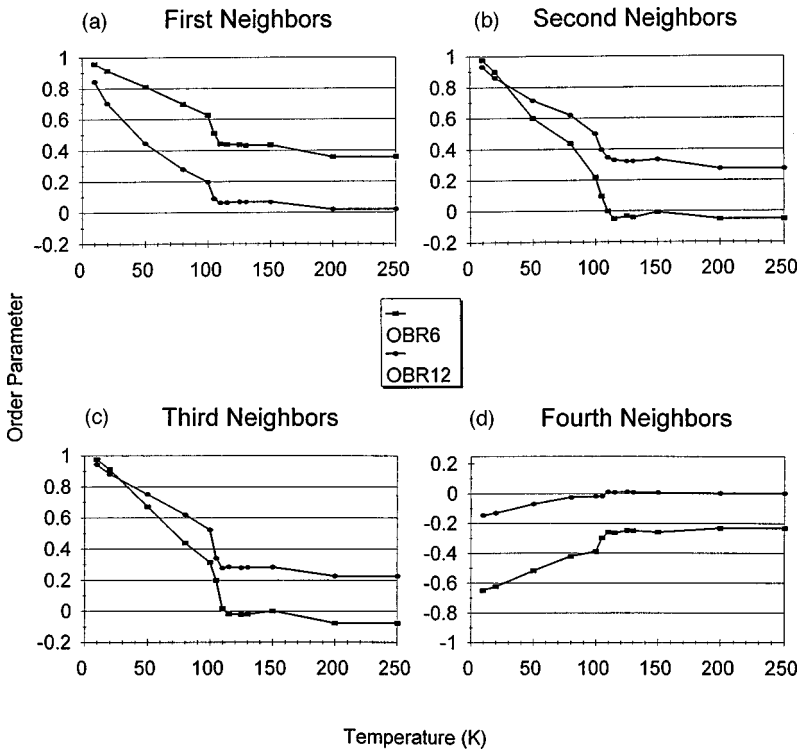

FIG. 3. Order parameters $OBR6$ and $OBR12$ as functions of temperature for first through fourth neighbors, respectively. Squares indicate $OBR6$ and circles indicate $OBR12$. Uncertainties are similar to those of $O1$ and $O2$. All points are connected by straight lines as a visual aid.

of occurrence of ϕ_{ij} for all atom pairs (i,j) between ϕ_{ij} and $\phi_{ij}+\Delta\phi_{ij}$ for $\Delta\phi_{ij}=0.002\pi$ in the interval $[0,2\pi]$. This bond-angle distribution is useful in that it signals $(2p)$-fold symmetry by peaks at $\phi_{ij}=(n\pi/p)+\beta$, where $n=1,2,\ldots,2p$ and β is a constant angle that may be thought of as the angle the shell is rotated with respect to the positive x axis.

Unnormalized bond-angle orientational distributions $P(\alpha_{ij})$ are shown at various temperatures for Kr/gr in Figs. 5(a)–5(j). $P(\alpha_{ij})$ is calculated using the same method as for $P(\phi_{ij})$. By virtue of its construction, this bond-angle distribution is able to signal the presence of local vacancies and interstitials in the neighbor shells, and is also useful in that it signals $(2p)$-fold symmetry in peaks at $\alpha_{ij}=\pi/p$. $P(\alpha_{ij})$ also is able to signal the presence of m consecutive vacancies in a given neighbor shell exhibiting $(2p)$-fold symmetry by peaks at $\alpha_{ij}=(m+1)\pi/p$ and m consecutive interstitials by peaks at $\alpha_{ij}=\pi/\{(m+1)p\}$. Here $m=1,2,\ldots,2p$; for single vacancies $m=1$.

Unnormalized pair-distribution functions $P(r_{ij})$ are shown at various temperatures for solid Kr/gr in Figs. 6(a)–6(e). $P(r_{ij})$ is calculated by determining the frequency of occurrence of r_{ij} for all atom pairs (i,j) between r_{ij} and $r_{ij}+\Delta r_{ij}$ for $\Delta r_{ij}=0.03$ Å in the interval [0 Å, 12 Å] and

TABLE II. Zero-temperature values, changes upon melting, and values at $T=250$ K for $OBRn$ with $n=1$, 2, 3, 4, 5, 6, and 12 for various neighbors presented in the same format as Table I. Uncertainties are of the same order as in Table I. Asterisks (*) denote that the order parameter has gradually approached zero throughout the solid phase and there is no sudden change in its value upon melting.

	$OBR1$	$OBR2$	$OBR3$	$OBR4$	$OBR5$	$OBR6$	$OBR12$
Zero-	0.5	−0.5	−1	−0.5	0.5	1	1
temperature	0.5	−0.5	−1	−0.5	0.5	1	1
value	0.5	−0.5	−1	−0.5	0.5	1	1
	0.857	0.479	0	−0.420	−0.653	−0.652	−0.15
Change	−0.019	0.077	0.172	0.054	0.147	−0.194	−0.128
upon	−0.020	*	0.133	0.060	*	−0.260	−0.179
melting	−0.046	*	0.175	0.097	*	−0.334	−0.239
	−0.085	−0.097	*	0.065	0.119	0.139	*
Value	0.482	−0.236	−0.604	−0.333	0.109	0.358	0.019
at	0.4024	−0.011	−0.193	−0.205	−0.138	−0.050	0.275
$T=250$ K	0.4712	0.0948	−0.077	−0.125	−0.122	−0.077	0.227
	0.7054	0.3051	0.026	−0.128	−0.207	−0.231	0.004

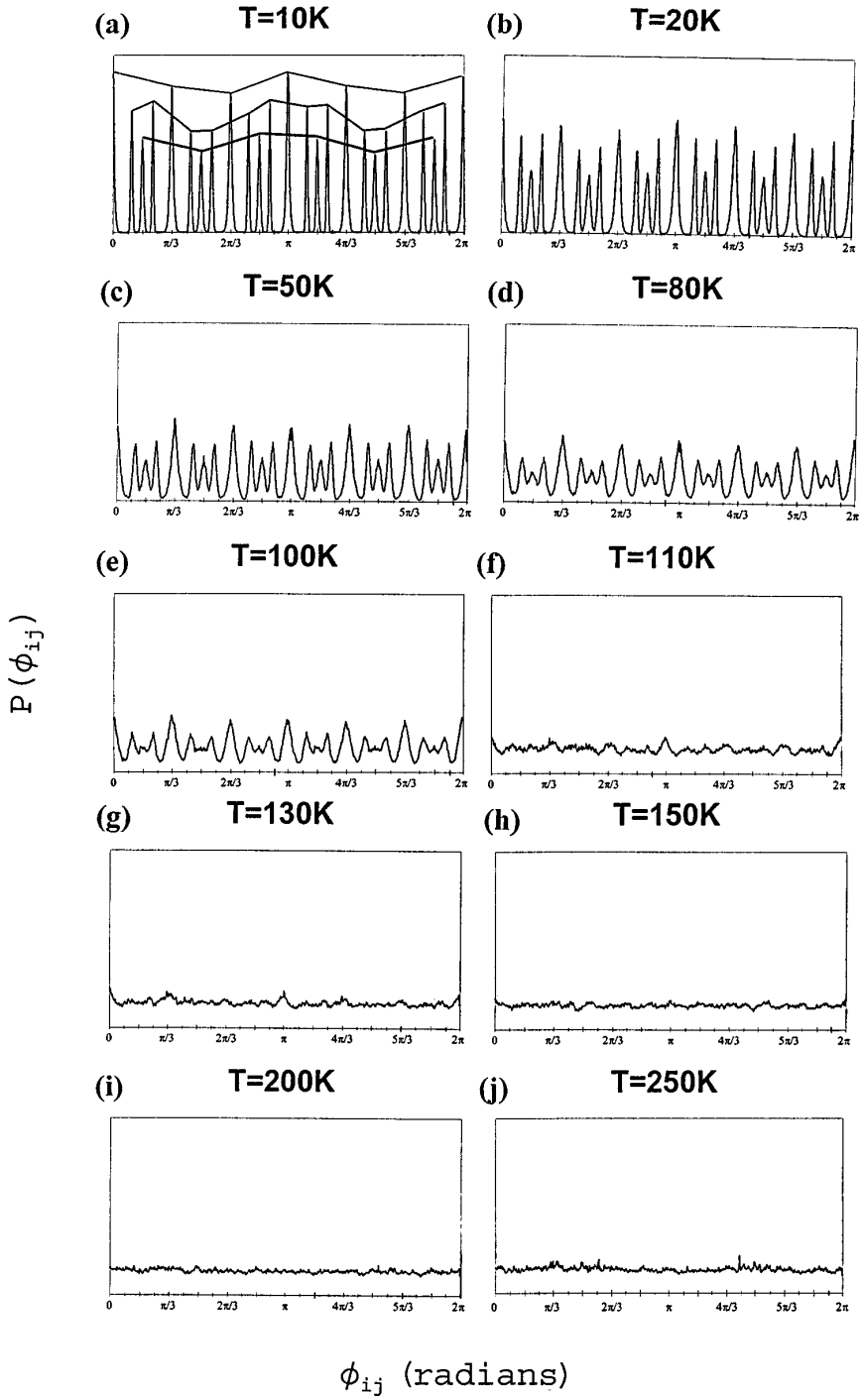

FIG. 4. Bond-angle distributions $P(\phi_{ij})$ over first through fourth neighbors collectively at various temperatures. The vertical scales are identical and arbitrary. In (a), light, medium, and heavy lines join the peaks for first and third (shared), fourth and second neighbors, respectively, to illustrate low-temperature modulation.

subsequently dividing by $2\pi r_{ij}\Delta r_{ij}$. Emphasis is placed on the temperature dependence of the second- and third-neighbor peaks.

After Udink and van der Elsken,[27] finite-size scaling is applied to the Kr/gr system in calculating the algebraic exponent η_6 for the orientational order parameter $OB6$. In an algebraically ordered phase, $|OB6| \sim L^{-\eta_6/2}$, where L is the system length. When η_6 becomes greater than its critical value of $\frac{1}{4}$, an orientationally ordered hexatic phase is unstable and should not exist. The system is divided into four subsystems with different sizes, and subsequently the logarithm of the order parameter is plotted against the logarithm of the system length at various temperatures and the values for η_6 are obtained from the slopes of the best linear fits to the data points.[27] The resulting algebraic exponents plotted at various temperatures are shown in Fig. 7.

IV. DISCUSSION

A. General remarks

Based on the behavior of $O1(T)$ and $O2(T)$ in conjunction with various thermodynamic quantities, the melting tem-

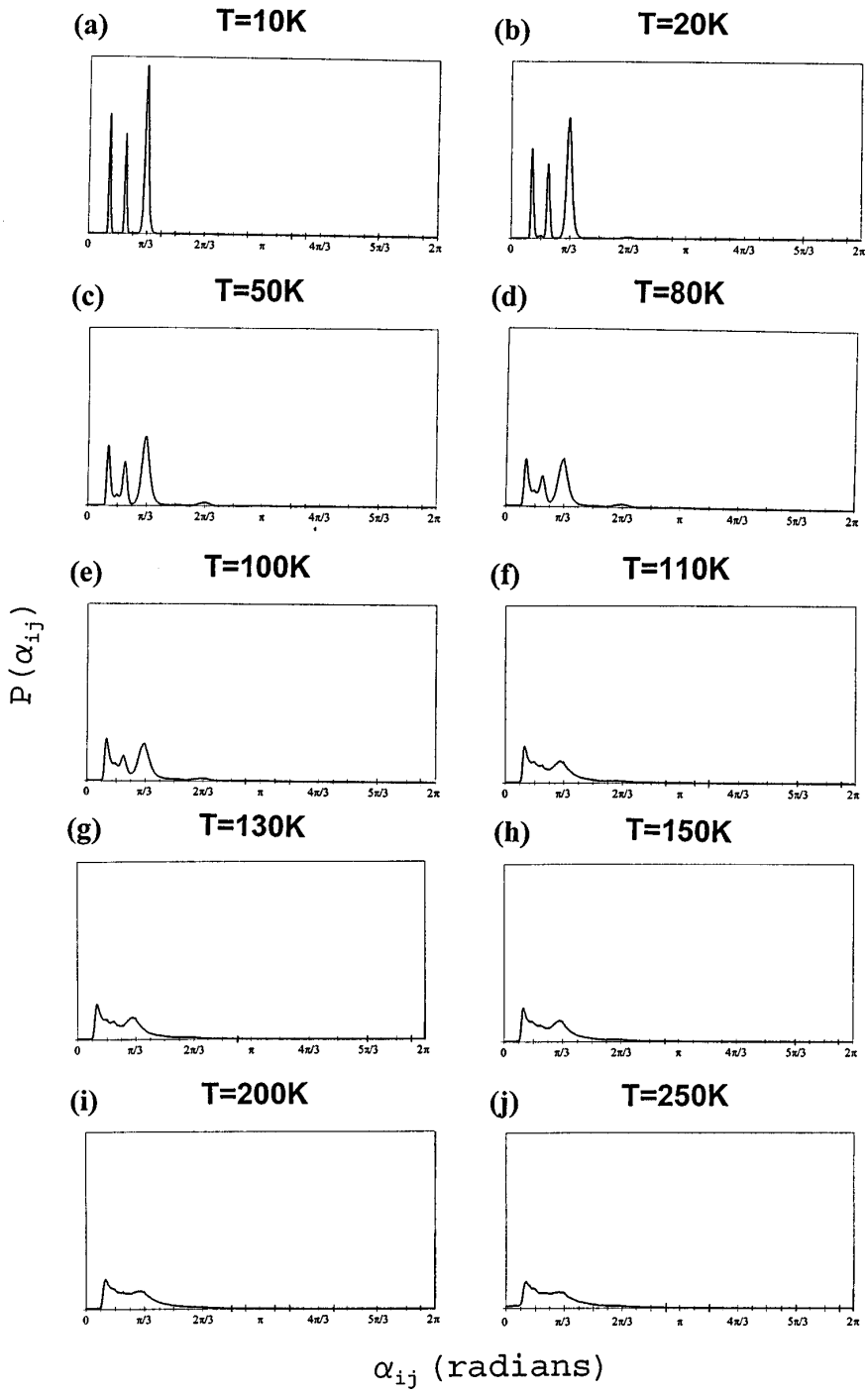

FIG. 5. Bond-angle distributions $P(\alpha_{ij})$ over first through fourth neighbors collectively at various temperatures. The vertical scales are identical and arbitrary.

perature is determined to be $T_m = 105 \pm 5$ K with the transition taking place over roughly a 25 K temperature range between 100 and 125 K. This is in good agreement with previous experimental and computational work.[22,23] The melting temperatures given by translational-order parameters as well as the bond-orientational parameters to be discussed are in agreement, testifying to the reliability of the statistics in the time averages. Effects of artificialities will be discussed later. For convenience, neighbor regimes are referred to as neighbor shells, dynamic as they may be.

Examination of the behavior of η_6, the algebraic exponent for $OB6$ as shown in Fig. 7 reveals that the critical value of $\eta_6 = \frac{1}{4}$ is reached close to $T = 100$ K, which coincides with the onset of structural and thermal melting. In larger Lennard-Jones systems[27] the translational-order algebraic exponents reached their critical value of $\frac{1}{3}$ significantly earlier than did the orientational exponents, indicating the presence of a temperature regime that could very well have been hexatic and was consistent with the KTHNY theory. In the Kr/gr system with this study, however, the coincidence of the loss of structural and orientational order points toward the conclusion that neither a hexatic phase nor an intermediate region between solid and fluid is supported in this system for this computational cell size, and therefore suggests that

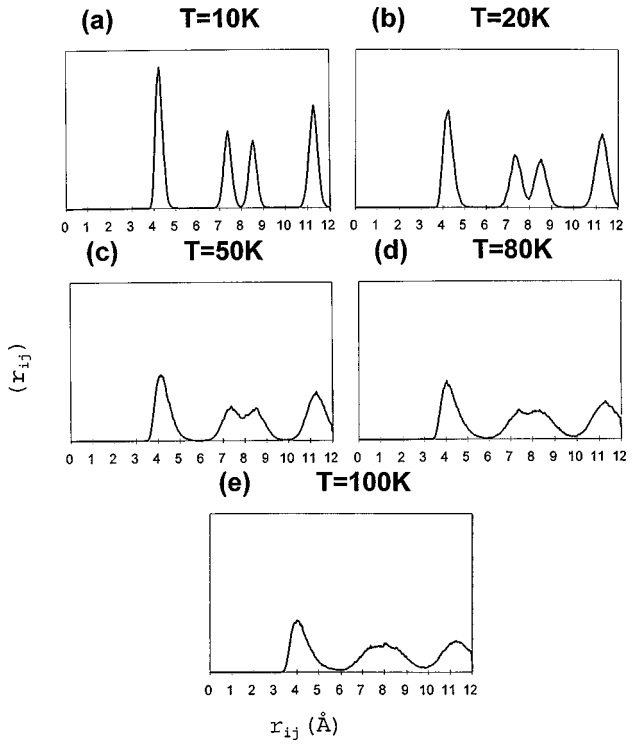

FIG. 6. Pair-distribution functions $P(r_{ij})$ over first through fourth neighbors collectively at various temperatures. The vertical scales are identical and arbitrary. Emphasis is on the behavior of the second peak and the function has been truncated at $r_{ij}=12$ Å.

the floating bond-orientational order seen in the fluid is not hexatic either. The contrasts of these results with those of Udink and van der Elsken[27] imply that a thorough study of the dependence bond-orientational order behavior on computational cell size is warranted in order to rule out a hexatic or intermediate phase with more confidence.

B. First neighbors

The first-neighbor shell has strong sixfold symmetry at low temperature ($T\approx 10$ K) both with respect to the substrate and intrinsically. This is evidenced by the behavior of the order parameters $OB6(T)$, $OB12(T)$, $OBR6(T)$, and $OBR12(T)$. In addition, the first-neighbor symmetry manifests itself as peaks in $P(\phi_{ij})$ at $\phi_{ij}=n\pi/3$ with

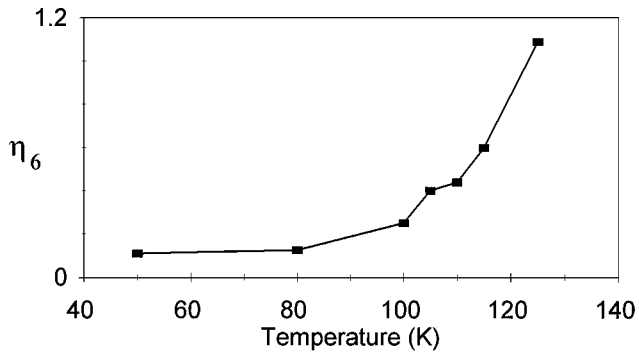

FIG. 7. Algebraic exponents η_6 for the orientational order parameter $OB6$ at various temperatures. Uncertainties are on the order of ± 0.05, and points are connected by straight lines as a visual aid.

$n=0,1,2,\ldots$, and a peak in $P(\alpha_{ij})$ for $\alpha_{ij}=\pi/3$. These peaks are also shared with the third-neighbor shell. Modulation is present in the first-neighbor peaks of $P(\phi_{ij})$ at low temperature, which are connected by the lightest lines in Fig. 4(a). This is due to the fact that the lateral corrugation in the adatom-substrate interaction energy is anisotropic. The anisotropy manifests itself in the modulation of groups of peaks in $P(\phi_{ij})$ corresponding to complete neighbor shells, with minima at $\phi_{ij}=\pi/2$ and $3\pi/2$ and maxima at $\phi_{ij}=0$, π, and 2π. Fluctuations in position are purely in the $\hat{x}$ direction for fluctuations in the former two angles and purely in the $\hat{y}$ direction for the latter three cases, which are not equivalent directions on the graphite substrate or on the Kr lattice. The modulation, however, disappears at $T\approx 50$ K which is consistent with the roughly 80 K lateral potential wells experienced by the adatoms due to the substrate periodicity. As heating of the solid takes place, thermal fluctuations ensue, causing $OB6$ and $OB12$ to decrease in value. The latter is substantially smaller than the former, as $OB12$ is more fluctuation sensitive. Upon melting, $OB6$ and $OB12$ both exhibit very large changes and subsequently drop to zero, as shown in Table I, indicating that the first-neighbor shell has lost bond-orientational order with respect to the substrate. In concert with translational-order loss, $P(\phi_{ij})$ flattens, as all angles for all neighbor shells become more uniformly sampled. $OB6$ and $OB12$ remain very small in the fluid phase, which also signals loss of bond-orientational order with respect to the substrate.

In the solid, $OBR6$ and $OBR12$ both decrease in magnitude due to thermal fluctuations. Upon melting, however, $OBR12$ drops to a little above zero while $OBR6$ experiences a much smaller change, dropping to a value substantially higher than zero. Although it is clear that some of the lattice bond-orientational order is lost across melting, it is also clear, from examining the $T=250$ K values for all $OBRn$ shown in Table II, that the first-neighbor shell retains sixfold floating bond-orientational order well into the fluid. $OB6$ and $OBR12$ maintain nonzero values in the fluid even through the beginning of desorption at $T\approx 200$ K. Those values are insensitive to changes in temperature, implying that vacancy generation does not significantly increase with increasing temperature in the fluid. However, these order parameters seem to show some slight changes when desorption ensues, which is consistent with the fact that $OBR6$ and $OBR12$ are sensitive to vacancies and interstitials. This sensitivity is apparent in the high-temperature behavior for second and third neighbors as well, but is not significant in the order parameters presented for fourth neighbors. It is also apparent that, from the behavior of $OBR6$, $OBR12$, and $P(r_{ij})$ that, in the first-neighbor shell, random thermal fluctuations without the significant interaction of other neighbor shells inducing defects are instrumental in structural order loss.

C. Second and third neighbors

The second-neighbor shell has low-temperature sixfold symmetry with respect to the adsorbate lattice, and sixfold symmetry with respect to the substrate that is rotated $\pi/6$ from the first-neighbor shell. This is evidenced by the behavior of $OB6$, $OB12$, $OBR6$, $OBR12$, and especially by the

fact that $OB6<0$ prior to approaching zero after melting. The second-neighbor shell's symmetry is reflected by peaks in $P(\phi_{ij})$ at $\phi_{ij}=(n+\frac{1}{2})\pi/3$ and by a peak of $P(\alpha_{ij})$ at $\alpha_{ij}=\pi/3$. In addition, third neighbors exhibit low-temperature sixfold symmetry with respect to both the adsorbate lattice and the substrate that is of the type similar to that for first neighbors. Order parameters and bond-angle distributions reflect this symmetry, and modulation of $P(\phi_{ij})$ peaks similar to that for first neighbors is also present and illustrated by the light lines shown in Fig. 4(a). In the low-temperature solid phase ($T\leqslant 10$ K), $OBR6\approx OBR12$ to within uncertainty, as shown in Fig. 3(c). However, at some temperature $20<T<50$ K, $OBR6$ diverges from $OBR12$ with $OBR12>OBR6$. As shown in Figs. 5 and 6, this divergence corresponds to the merging of the second and third peaks of the pair-distribution function, and hence marks the beginning of dynamic interactions between the second- and third-neighbor shells. In addition to the $OBRn$ behavior, it is striking to note that, for all T examined, $|OB6|\approx|OB12|$; they do not exhibit the above-mentioned divergence for these neighbor shells and $OBR6$ vanishes for the fluid. The combination of the three preceding observations supports the notion that random fluctuations are not the only avenues responsible for thermal decay of structural order in the solid. If they were, surely it would stand to reason that $|OB6|>|OB12|$ and $OBR6>OBR12$ for all T prior to melting, since we have the constraint that both shells initially display sixfold symmetry at low temperature. Examination of $P(\alpha_{ij})$ shows emerging peaks in $P(\alpha_{ij})$ at $\alpha_{ij}=\pi/6$ and at $\alpha_{ij}=2\pi/3$ for $T=20$ K and more pronounced peaks for $T=50$ K. This, combined with the behavior of OBn and $OBRn$, suggest that, beginning with the divergence of $OBR6$ with respect to $OBR12$, the second- and third-nearest neighbor shells are exchanging atoms thereby creating paired lattice defects in the form of local interstitials and vacancies. This behavior occurs through melting and into the fluid at $T\approx 250$ K, as evidenced by the behavior of $P(\alpha_{ij})$ and $P(r_{ij})$. In this regime, however, Tables I and II, as well as Figs. 2(a)–2(d) and 3(a)–3(d) show that, just as for the first-neighbor shell, all bond-orientational order with respect to the substrate is lost, but floating bond-orientational order persists into the high-temperature fluid. By examining the change upon melting and the $T=250$ K values for the $OBRn$ in Table II, it is clear that the bond-orientational order is dynamic in nature and not just static 12-fold symmetry. In the high-temperature fluid, $P(\alpha_{ij})$ appears to show a sharp barrier to any $\alpha_{ij}<\pi/12$ as well as decaying probability for occurrence of $\alpha_{ij}>\pi/3$. The former may be understood that, within the context of the construction of this probability distribution, this is analogous to the sharp barrier before the first peak of the pair-distribution function and is related to the steep Kr-Kr potential barrier for close-pair separation. The latter indicates that not only are paired lattice defects present in the system, but significant random thermal fluctuations as well. Complete coverage offers the constraint that not many local vacancies may be created in a given neighbor shell due to steric considerations; therefore as α_{ij} increases, reflecting a larger population of local vacancies, the probability of their occurrence decreases significantly. Therefore, neighbor shells seldom experience multiple consecutive vacancies or interstitials.

D. Fourth neighbors

The fourth-neighbor shells are the first shells outward that do not exhibit strong sixfold symmetry. They contribute peaks to $P(\phi_{ij})$ at roughly $\phi_{ij}=(1+3n)\pi/9$ and at $\phi_{ij}=(2+3n)\pi/9$, and to peaks of $P(\alpha_{ij})$ at about $\alpha_{ij}=\pi/9$ and at $\alpha_{ij}=2\pi/9$. As for first through third neighbors, the peaks of $P(\phi_{ij})$ for fourth neighbors are also modulated, as shown in Fig. 4(a) by the medium lines connecting the appropriate peaks. All OBn and $OBRn$ show a gradual decline of structural order and symmetry upon heating of the solid. $OBR12$ falls to zero in the solid because it is fluctuation sensitive, but $OBR3$ remains close to zero due to the inherent symmetry of the neighbor shell. Of all the neighbor shells, the fourth-neighbor shells exhibit the most gradual changes overall upon melting, by examination of not only the $OBRn$ and their changes upon melting, but also of their $T=250$ K values as compared to their zero-temperature values as shown in Table II. This supports the concept that long-range fluctuations are instrumental in more continuous transitions. Although all OBn go to zero upon melting and remain zero in the fluid, the $OBRn$ signal substantial floating bond-orientational order possessed at high temperature by the fourth-neighbor shell, as $OBRn$ for $n=1$, 2, 4, 5, and 6 have nonzero values for the high-temperature fluid.

E. Effects of artificialities

One of the most important effects to monitor in any computational endeavor is that of the finite computational cell size and boundary conditions on the simulation results. In agreement with Novaco's work with pinned-edge atoms,[28] the melting temperature for Kr/gr increases dramatically when reflection boundary conditions (RBC's) are utilized, by about 10 K for $N=256$ to 35 K for $N=16$. Of course, this underscores the relative unimportance of the boundary as the system size increases. More importantly, and central to the present work, as computational cell size decreases, especially with RBC's, the bond-orientational order is seen to persist into the fluid phase more, even to the point that, with $N=16$, $P(\phi_{ij})$ at $T=250$ K exhibits distinct peaks and valleys similar to the distribution right after melting. This is consistent with the phase transition ''blurring'' exhibited by small computational cells. The small system size yields results in the order parameters generally consistent with those for larger systems, but artificially preserved bond-orientational order in the fluid as the computational cell size is decreased. Some simulations were completed in which the undulation of the interaction due to the graphite periodicity is removed, and the bond-orientational behavior is virtually identical to the case where the undulation is included. For no system size examined did the floating bond-orientational order disappear, and hence the fundamental results of the present work are felt to be reliable. However, the study done here clearly indicates that an exhaustive examination of the dependence of the bond-orientational behavior on computational cell attributes is warranted.

V. CONCLUSIONS

The major conclusions of this work are as follows.

(i) In Kr/gr the first-neighbor shell exhibits strong sixfold

symmetry in the low-temperature solid phase ($T \approx 10$ K). In the heating of the solid, random thermal fluctuations without vacancy/interstitial generation induced by interaction with other neighbor shells are mainly responsible for the decay of structural order. Upon melting, the adsorbate loses all bond-orientational order with respect to the substrate but retains floating bond-orientational order well into the fluid.

(ii) The second- and third-neighbor shells exhibit random thermal fluctuations with increasing mutually supported generation of vacancy/interstitial pairs, becoming prominent at some temperature $20 < T < 50$ K coincident with the merging of the two neighbor shell peaks of the pair-distribution function and the divergence of $OBR6$ with respect to $OBR12$. Melting proceeds with the lattice defects active, and floating bond-orientational order persists well into the fluid.

(iii) The fourth-neighbor shells exhibit random thermal fluctuations in the solid without significant vacancy/interstitial generation through interaction with other neighbor shells that persist into the high-temperature fluid. The shell never exhibits strong sixfold or 12-fold symmetry, and melting signatures are relatively weak, consistent with a more continuous transition dominated by long-range fluctuations. Floating bond-orientational order persists well into the fluid for this shell also.

(iv) In the solid the anisotropic lateral corrugation of the adsorbate-graphite potential interaction modulates the bond-angle distribution $P(\phi_{ij})$, but the modulation disappears as the temperature is raised to $T \approx 50$ K.

(v) Temperature increase has little effect on the floating bond-orientational order of any neighbor shell in the fluid phase. Therefore, heightened vacancy promotion in the fluid through increasing temperature is insignificant, as $OBR6$ and $OBR12$ are vacancy sensitive by virtue of their construction. However, at $T \approx 200$ K a slight change is noted in the order parameters for the first three neighbor shells when desorption begins, as more vacancies are formed.

(vi) The computational cell size and boundary conditions have an effect on the bond-orientational order with respect to the substrate, which is artificially exaggerated for smaller systems. The floating bond-orientational order observed in Kr/gr does not seem to be an artifact of system size, but further detailed investigation is certainly warranted.

(vii) Based on behavior of various bond-angle distributions, the likelihood of consecutive multiple vacancies or interstitials present in a given neighbor shell is far less than for single ones.

(viii) Based on the behavior of the algebraic exponent η_6 for $OB6$, there is no significant temperature regime where a hexatic phase or intermediate region is supported in this system, but further studies with larger computational cell sizes could be helpful in resolving the issue.

ACKNOWLEDGMENTS

This work has been supported by a grant from Texas A&M International University, and from computer-time-allocation grants from Texas A&M at College Station.

[1] W. F. Brinkman, D. S. Fisher, and D. E. Moncton, Science **217**, 693 (1982).
[2] K. J. Strandburg, Rev. Mod. Phys. **60**, 161 (1988).
[3] J. M. Kosterlitz and D. J. Thouless, J. Phys. C **6**, 1181 (1973).
[4] J. M. Kosterlitz, J. Phys. C **7**, 1096 (1974).
[5] B. I. Halperin and D. R. Nelson, Phys. Rev. Lett. **41**, 121 (1978).
[6] D. R. Nelson and B. I. Halperin, Phys. Rev. B **19**, 2457 (1979).
[7] F. F. Abraham, Phys. Rep. **80**, 339 (1981).
[8] R. Marx, Phys. Rep. **125**, 1 (1985).
[9] Juan J. Morales, Phys. Rev. E **49**, 5127 (1994).
[10] Juan J. Morales, Enrique Velasco, and Soren Toxvaerd, Phys. Rev. E **50**, 2844 (1994).
[11] R. E. Kusner, J. A. Mann, J. Kerins, and A. J. Dahm, Phys. Rev. Lett. **73**, 3113 (1994).
[12] Kun Chen, Theodore Kaplan, and Mark Mostoller, Phys. Rev. Lett. **74**, 4019 (1995).
[13] Jun Hu and A. H. MacDonald, Phys. Rev. Lett. **71**, 432 (1993).
[14] Kevin Naidoo and Jurgen Schnitker, Mol. Phys. **80**, 1 (1993).
[15] J. A. Zollweg, *Ordering in Two Dimensions* (Elsevier North-Holland, Amsterdam, 1980), p. 331.
[16] J. P. McTague, D. Frenkel, and M. P. Allen, *Ordering in Two Dimensions* (Elsevier North-Holland, Amsterdam, 1980), p. 147.
[17] H. Weber and D. Marx, Europhys. Lett. **27**, 593 (1994).
[18] Keiko M. Aoiki and Fumiko Yonezawa, Phys. Rev. Lett. **69**, 2780 (1992).
[19] E. Gorecka, Li Chen, O. Lavrentovich, and W. Pyzuk, Europhys. Lett. **27**, 507 (1994).
[20] Gernot A. Overbeck, Dirk Hönig, Lydia Wolthaus, Michael Gnade, and Dietmar Möbius, Thin Solid Films **242**, 26 (1994).
[21] R. Seshardi and R. M. Westervelt, Phys. Rev. Lett. **66**, 2774 (1991).
[22] N. D. Shrimpton, M. W. Cole, and W. A. Steele (private communication).
[23] E. D. Specht, A. Mak, C. Peters, M. Sutton, R. J. Birgenau, K. L. D'Amico, D. E. Moncton, S. E. Nagler, and P. M. Horn, Z. Phys. B **69**, 347 (1987).
[24] N. Dupont-Pavlovsky, C. Bockel, and A. Thomy, Surf. Sci. **160**, 12 (1985).
[25] R. G. Caflisch, A. N. Berker, and M. Kardar, J. Vac. Sci. Technol. A **3**, 1592 (1985).
[26] W. A. Steele, Surf. Sci. **36**, 317 (1973).
[27] C. Udink and J. van der Elsken, Phys. Rev. B **35**, 279 (1987).
[28] A. D. Novaco, Phys. Rev. B **35**, 8621 (1987).